Turkish Journal of Electrical Engineering & Computer Sciences

http://journals.tubitak.gov.tr/elektrik/

Research Article

Turk J Elec Eng & Comp Sci
(2023) 31: 969 – 991

doi:10.55730/1300-0632.4029

Enhancing exploration-exploitation in harmony search for airborne hyperspectral imaging band selection (E3HS)

Mohammed Abdulmajeed MOHARRAM, Divya Meena SUNDARAM*
School of Computer Science and Engineering, VIT-AP University, Amaravati, Andhra Pradesh, India

Received: 24.04.2023 • **Accepted/Published Online:** 20.08.2023 • **Final Version:** 27.10.2023

Abstract: Hyperspectral imaging has emerged as a prominent area of research in the field of remote sensing science. However, hyperspectral images (HSIs) pose a notable challenge due to the presence of numerous irrelevant and redundant spectral bands exhibiting high correlation. Therefore, it is necessary to enhance the classification performance for HSI processing by selecting the most relevant discriminative spectral bands. To this end, this paper introduces a metaheuristic search method called enhancing exploration-exploitation in harmony search (E3HS). The standard harmony search suffers from many weaknesses, such as premature convergence and falling easily into the local optimum. Consequently, E3HS was proposed to evade falling into the local optimum by creating a balance between exploration and exploitation strategies to accelerate convergence toward the global optimum solution. Finally, two machine learning classifiers (k-nearest neighbor and support vector machine) were employed for hyperspectral image classification at the pixel level. Moreover, the proposed method was compared with the bat algorithm, Archimedes optimization algorithm, particle swarm optimization, standard harmony search, genetic algorithm, and krill herd algorithm. The experimental results demonstrated significant improvement with overall accuracy equal to 87.49%, 94.85%, and 94.41% for the Indian Pines, Pavia University, and Salinas datasets, respectively.

Key words: Metaheuristic algorithm, exploration, exploitation, band selection, fitness function

1. Introduction

Hyperspectral imaging captures rich and discriminative information that enables the differentiation of chemical and physical characteristics within regions of interest [1]. Hyperspectral images (HSIs) contain hundreds of adjacent spectral bands that span the electromagnetic spectrum and can accurately distinguish similar objects [2]. Moreover, HSIs consist of three dimensions, with two dimensions describing the spatial features and the third dimension representing the spectral features [3]. Furthermore, hyperspectral imaging has been widely utilized across various disciplines, showcasing its versatility and potential for numerous applications such as precision agriculture [4], environmental monitoring [5], mineral exploration [6], biomedical imaging [7], and archaeology [8]. However, the rich spectral information provided by HSIs presents both opportunities and challenges. On the one hand, it allows for detailed analysis and identification of materials based on their unique spectral signatures. On the other hand, the high dimensionality of hyperspectral data poses computational and analytical complexities, requiring advanced processing techniques for effective interpretation and classification [9]. Therefore, the process of HSI dimensionality reduction plays a crucial role in achieving high accuracy, reducing computational complexity, and mitigating the Hughes phenomenon. By extracting the most informative and discriminative

*Correspondence: divyameena.s@vitap.ac.in

spectral features, dimensionality reduction techniques enable more efficient data analysis, improved classification performance, and better utilization of computational resources. The methods for HSI dimensionality reduction can be classified into two main categories: feature extraction approaches and feature selection approaches [10]. Feature extraction approaches aim to transform the original high-dimensional HSI data into a lower-dimensional representation by extracting a set of new features that capture the most relevant information. Some commonly used feature extraction techniques for HSI include principal component analysis (PCA) [11], independent component analysis (ICA) [12], and minimum noise fraction (MNF) [13]. These methods focus on finding a new representation of the data that preserves the most discriminative spectral characteristics while reducing the dimensionality. Moreover, deep learning models have been recently applied for feature extraction by learning discriminative features from the input data and capturing both local and global spectral information, as well as spatial dependencies [14]. Unlike feature extraction methods, feature selection (band selection) approaches aim to select a subset of the original spectral bands that are most informative and relevant for the classification task [15]. These methods evaluate the importance or relevance of each spectral band and retain only the most discriminative ones. Popular feature selection techniques for HSI include sequential forward selection (SFS) [16], sequential backward selection (SBS) [17], and mutual information-based methods [18,19]. By selecting a subset of spectral bands, feature selection approaches reduce the computational complexity and enhance classification performance by eliminating irrelevant and redundant information. Moreover, band selection methods are generally performed to select the most informative and relevant spectral bands while keeping the original band's discriminatory information and maintaining meaningful physical information for the HSI. According to the availability of class labels, the methods for selecting spectral bands are classified into two types: supervised and unsupervised methods [20]. Supervised methods rely on the class label information to choose the best informative bands [21]. On the contrary, unsupervised methods do not depend on preliminary information related to the class labels to select the most discriminant bands [22]. Moreover, several approaches have been implemented to specify meaningful bands, such as clustering-based approaches and ranking-based approaches [23]. As for band selection based on clustering methods, it mainly comprises two steps. In the first step, the spectral bands are assembled into clusters where the intercluster variance will be maximized between bands in the other cluster and the intracluster variance will be minimized between bands in the same cluster. Then, in the second step, the best spectral bands with the highest average correlations are selected from the corresponding clusters [24]. Despite clustering-based methods being widespread methods in selecting meaningful spectral bands, some significant and relevant bands are still neglected when choosing spectral bands due to clustering-based methods depending mainly on redundancy between bands. On the other hand, ranking-based techniques are performed by ranking all the spectral bands according to a specific evaluation measure. The spectral bands are then arranged according to the top-ranked and, ultimately, the subset of the spectral bands of the top-ranked is formed [25]. However, in some cases, ranking-based methods select redundant bands because the correlation between bands is not considered while evaluating and ranking the bands. Although many previous techniques have been introduced for choosing the most relevant discriminative spectral bands, it still represents a significant dilemma.

Additionally, nature-inspired optimization approaches have been utilized to select the most informative spectral bands, such as artificial bee colony (ABC) [26], genetic algorithms (GAs) [27], particle swarm optimization (PSO) [28], the bat algorithm (BA) [29], and wind-driven optimization (WDO) [30]. Table 1 presents a literature review for HSI band selection using different optimization methods. Furthermore, metaheuristic optimization algorithms consider the optimization problem as a spectral band selection problem addressed by

effectively defining the appropriate fitness function [31]. The selected bands' effectiveness is evaluated and their quality is measured via the fitness function. Therefore, it is essential to carefully define the fitness function as it affects the overall performance. Moreover, many evaluation measures can be considered as fitness functions, such as distance criteria based on calculating the distance between selected spectral bands (Bhattacharya distance or Hausdorff distance) [32], information measurement criteria (the entropy criterion or mutual information) [33], and dependency criteria (measuring similarity and correlations between spectral bands) [34]. In addition, selecting an effective optimization algorithm is also a significant factor in selecting discriminant spectral bands effectively. A suitable optimization algorithm should be chosen, leading to convergence towards the global optimum solution, avoiding premature convergence or falling into the local optimum [35]. Many previous studies have been conducted for selecting the most informative spectral bands of hyperspectral images using optimization algorithms such as GAs inspired by Darwin's theory. However, comparing GAs with the standard harmony search (HS), we find that the HS considers all the solutions in the harmony memory (HM) to generate the new solution, unlike GAs, which depend on only two solutions (parents) to generate the new solution [36]. However, despite the HS algorithm being much faster than GAs in terms of execution time, the HS cannot reach the optimal solution effectively, and it suffers from premature convergence and falling into the local optimum easily. In this paper, HSI dimensionality reduction is addressed by selecting the most informative spectral bands. The HSI also contains a large number of irrelevant and noisy spectral bands that need to be removed in order to reduce the processing time and eliminate the Hughes phenomenon. The HS is used for selecting the most important spectral bands as it requires less computation time compared to many optimization algorithms. However, the HS algorithm suffers from some shortcomings such as easily falling into the local optima and premature convergence. In order to address all of these problems, the main contributions of this study are as follows:

1. This study introduces an enhanced version of the HS algorithm specifically designed for selecting the most relevant and informative spectral bands. By effectively reaching the global solution within the search space, the algorithm ensures that the selected bands are highly discriminative and valuable for subsequent analysis tasks.

2. The proposed algorithm incorporates two additional solutions, referred to as harmonies, to further improve the band selection process. The first harmony leverages the worst individual experiences. Conversely, the second harmony exploits the best individual experiences of all harmonies. These improvisations enhance the algorithm's ability to balance exploration and exploitation strategies.

3. To evaluate the effectiveness of the proposed method, a comparative analysis is conducted with several well-known algorithms, including the bat algorithm (BA), Archimedes optimization algorithm (AOA), particle swarm optimization (PSO), harmony search (HS), genetic algorithm (GA), and krill herd (KH). The comparison is performed on three benchmark datasets commonly used in HSI analysis. The results demonstrate the remarkable superiority of the proposed method over the state-of-the-art band selection approaches.

This paper is arranged in the following form: Section 2 offers a brief overview of the HS algorithm, followed by the proposed methodology in Section 3, and the experimental results are outlined in Section 4. A discussion is presented in Section 5 and conclusions are drawn in Section 6.

Table 1. Literature review for HSI band selection using optimization methods.

References	Dataset	Optimization method	Year	Overall accuracy (OA)
[37]	Indian Pines	Gray wolf optimizer	2015	OA = 73.67%
	Pavia University			OA = 88.17%
	Salinas			OA = 95.38%
[38]	Indian Pines	Artificial bee colony	2020	OA = 78.07%
	Pavia University			OA = 90.56%
	Salinas			OA = 92.22%
[39]	Indian Pines	Improved whale optimization	2021	OA = 99.44%
	Pavia University			OA = 99.86%
	Salinas			OA = 99.83%
[40]	Indian Pines	Krill herd	2022	OA = 96.54%
	Pavia University			OA = 98.93%
	Salinas			OA = 99.78%
	Botswana			OA = 98.66%
[41]	Indian Pines	Moth–flame optimization	2022	OA = 88.98%
	Pavia University			OA = 94.85%
	Salinas			OA = 97.17%
[42]	Indian Pines	Multimodal evolutionary algorithm	2023	OA = 81.43%
	Pavia University			OA = 92.59%
	Salinas			OA = 93.51%

2. Harmony search

HS is a metaheuristic algorithm proposed by Geem in 2001 [43]. It relies on a musical improvisation strategy by improvising a new harmony to reach the optimal harmony by updating the harmony memory (HM) upon getting a harmony better than the worst harmony in the HM. Moreover, HS is characterized by its ability to generate a new solution by considering all the solutions in the HM, while a GA depends on only two solutions: the first and the second parent. Investigations also indicate that HS is better than GAs in terms of time [44]. Furthermore, HS has been employed in various scientific fields. The main steps of the HS method can be briefly explained as follows:

Step 1: The optimization problem and all parameters are initialized in this step. The primary objective of identifying the optimization problem is to maximize or minimize the fitness function (objective function). The main parameters are harmony memory size (HMS), harmony memory considering rate (HMCR), pitch adjusting rate (PAR), maximum iterations (the total number of iterations for improvising new harmony), and bandwidth (BW).

Step 2: The HM is initialized via Eq. (1) by generating solutions randomly between the lower and the upper bounds, and then the harmonies are arranged according to their fitness function.

Assuming that $HM = [X_1, X_2, .., X_z]$, $z = HMS$, and $X_i = (x_{i1}, x_{i2}, .., x_{id})$, where i=1,2,....., HMS, d represents the dimension of harmony (solution).

$$x_{iz} = Lb_z + R * (Ub_z - Lb_z) \tag{1}$$

Here, x_{iz} is the zth harmony vector in X_i; Lb_z and Ub_z represent the lower and the upper bounds, respectively; and R represents a random number between [0, 1].

Step 3: A new solution is improvised from the HM by considering three significant factors: memory consideration (MC), pitch adjustment (PA), and random selection (RS). A new candidate improvisation procedure is presented in Algorithm 1.

Step 4: Updating the HM: if the new solution has a fitness function value better than the worst fitness function

value in the HM, then the new solution is combined into the HM.

Step 5: Checking the stop condition: if the maximum number of new harmony improvisations is met, then the best solution with the best fitness function in the HM is returned; otherwise, steps 3 and 4 are repeated.

Algorithm 1 `Improvising new harmony.`

for `i = 1 to d:` **do**
  if `RAND1 <= HMCR` **then** % Memory Consideration
    $x_{newz} = x_{ranz}$; $Where\, ran \in (1, 2, 3, ..., HMS)$
    if `RAND2 <= PAR` **then** % Pitch Adjustment
      $x_{newz} = x_{newz} \mp RAND3 * BW$
    end if
  else
    $x_{newz} = Lb_z + RAND4 * (Ub_z - Lb_z)$; $Where\, RAND1, RAND2, RAND3, RAND4 \in [0, 1]$
  end if
end for

3. Proposed methodology

The enhancing exploitation-exploration in harmony search (E3HS) algorithm is proposed here to choose the most discriminative spectral bands for HSIs. The HSI is defined by $X \in R^{A*B*C}$, where A and B signify height and width, respectively, and C indicates the total number of bands. Moreover, the HS algorithm suffers difficulty in reaching the best solution within the search space due to premature convergence and quickly falling into the local optimum. Therefore, the HS algorithm has been enhanced by generating two additional harmonies in the standard HS algorithm. This section illustrates the primary objective of adding the two extra harmonies in addition to the fitness function used to select the most informative spectral band.

3.1. Enhancing search capability

The HS algorithm has been employed to solve many optimization problems effectively. However, the standard HS suffers from some weaknesses such as premature convergence and falling into local optima easily. Therefore, E3HS is introduced to handle those issues and improve the search capability to reach the global solution within the search space efficiently. The search capability is enhanced to select the most informative discriminative spectral bands according to the fitness function (classification performance) by improvising two additional solutions (harmonies). Moreover, the best and worst individual experiences of all harmonies in the HM are exploited to reach a global solution. More specifically, the first harmony enhances the global search (exploration) for harmonies by maintaining the worst individual experiences of all the harmonies in each iteration and then calculating the mean of all the worst individual experiences in the HM to generate the first harmony. Eq. (2) pertains to the first harmony. The first harmony will be added to the HM if it has a cost function value better than the worst cost function value in the HM. Moreover, the first harmony aims to maintain diversity, discover new possibilities of the most informative spectral bands within the search space, and avoid premature convergence. Figure 1 illustrates the mechanism for creating the first harmony.

$$x_{new2z} = x_{new2z} \mp \alpha * R1 * Mean(WorstHar) \tag{2}$$

On the other hand, the second harmony enhances the local search (exploitation) for harmonies by maintaining the best individual experiences of all harmonies in each iteration and then calculating the mean of

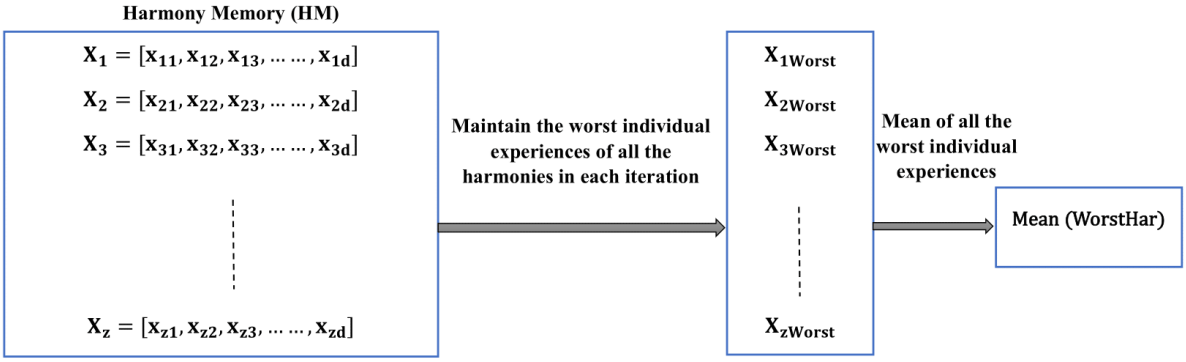

Figure 1. Mechanism to create the first harmony.

all the best individual experiences in the HM to generate the second harmony. Eq. (3) pertains to the second harmony.

$$x_{new3z} = x_{new3z} \mp \alpha * R2 * Mean(BestHar) \tag{3}$$

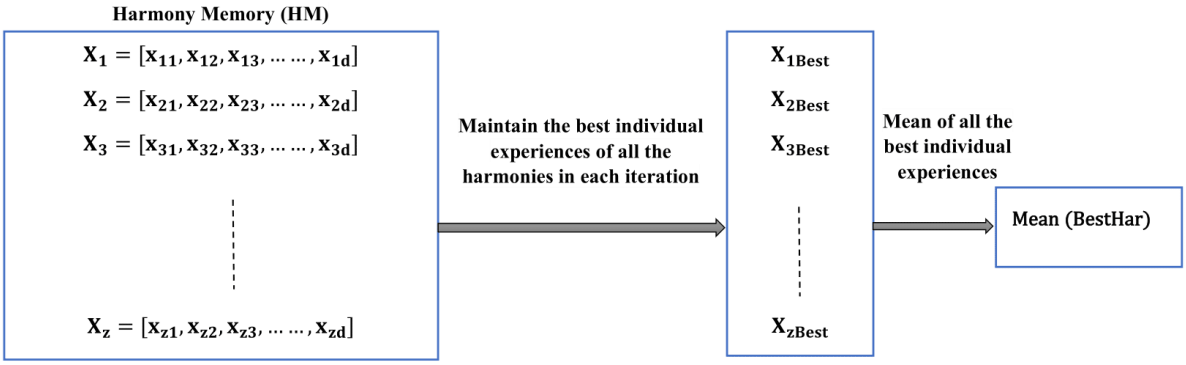

Figure 2. Mechanism to create the second harmony.

Here, $\alpha = 0.1$ indicates a constant value. R1 and R2 represent the random value within [0,1]. Mean (WorstHar), and Mean (BestHar) define the mean of all the worst and best individual experiences in the HM, respectively. The second harmony will also be added to the HM if the second solution has a cost function value better than the worst cost function value in the HM. Moreover, the second harmony aims to accelerate the convergence toward the optimal solution by considering the best individual experiences. Figure 2 illustrates the mechanism to create the second harmony. The primary purpose of generating two harmonies is to improve the search capability toward the optimal solution by selecting the most informative spectral bands. Consequently, E3HS can avoid falling into the local optimum by balancing the exploration and exploitation search and reaching the optimal global solution within the search space effectively.

3.2. Fitness function

The E3HS algorithm identifies the optimization problem by maximizing the fitness function. In other words, the relevant and significant spectral bands are selected, which maximizes the cost function. Moreover, the primary objective of this study is to reduce the HSI dimensions by selecting the lowest possible number of meaningful

Table 2. Main parameters of the proposed method and state-of-the-art methods.

Optimization method	Parameter	Value
BA	Loudness constant	0.97
	Emission rate constant	0.1
	Minimum frequency	0
	Maximum frequency	1
	Population size	5
	Maximum iterations	100
AOA	K1 (position constant)	2
	K2 (position constant)	1
	Upper range	0.9
	Lower range	0.1
	Population size	5
	Maximum iterations	100
PSO	Inertia weight	0.9
	Cognitive coefficient	2
	Social coefficient	2
	Population size	5
	Maximum iterations	100
HS	HMCR	0.95
	PAR	0.25
	BW	1
	HMS	5
	Maximum iterations	100
GA	Crossover rate	0.4
	Mutation rate	0.2
	Population size	5
	Maximum iterations	100
KH	Maximum speed	0.5
	Foraging speed	0.5
	Maximum diffusion speed	0.5
	Population size	5
	Maximum iterations	100

spectral bands with the highest fitness function. Assume that t number of classes for HSIs are indicated as $C = [c_1, c_2, c_3, , c_t]$. Furthermore, subset k of the selected spectral bands is shown as $B = [b_1, b_2, b_3, , b_k]$, so the fitness function (classification accuracy) is defined as in Eq. (4).

$$F(B) = \sum_{i=1}^{|A*B|} Check(p_i)/P \tag{4}$$

Here, P represents the whole number of pixels, and pixel p_i is evaluated through the classification process by checking whether the pixel classification is correct. In addition, if a pixel classification is an actual class, then (1) is assigned; otherwise, (0) is assigned, as in Eq. (5).

$$Check(p_i) = \begin{cases} 1, & \text{if } Classify(p_i) = C \\ 0, & \text{otherwise} \end{cases} \tag{5}$$

The selection of significant spectral bands using E3HS is illustrated by Algorithm 2. Table 2 defines the main parameters of the proposed method and the state-of-the-art methods. Moreover, the workflow of the proposed method for selecting meaningful spectral bands is displayed in Figure 3.

Algorithm 2 Spectral band selection using enhancing exploration-exploitation in harmony search (E3HS).

Input: Hyperspectral data X.

Output: Subset of the most significant and relevant spectral bands.

Initialize all parameters of the algorithm: maximum improvisations (MI), HMS, HMCR, PAR, BW, Lb, and Ub.
Initializes harmonies in the HM as well as the best individual experiences (BestHar) and the worst individual experiences (WorstHar) of harmonies by generating unique random integer values.
while iteration < = maximum improvisations (MI) **do**
  for i = 1 to d: **do**
    if RAND1 <= HMCR **then** % Memory Consideration
      $x_{newz} = x_{ranz}$; $Where\, ran \in (1, 2, 3, ..., HMS)$.
      if RAND2 <= PAR **then** % Pitch Adjustment
        $x_{new1z} = x_{new1z} \mp RAND3 * BW$.
        $x_{new2z} = x_{new2z} \mp \alpha * RAND4 * Mean(WorstHar)$.
        $x_{new3z} = x_{new3z} \mp \alpha * RAND5 * Mean(BestHar)$.

      end if
    else
      $x_{new1z} = URI1(Lb, Ub)$.
      $x_{new2z} = URI2(Lb, Ub)$.
      $x_{new3z} = URI3(Lb, Ub)$ where URI1, URI2, and URI3 are unique random integer values between (Lb, Ub).
    end if
  end for
  Calculate the fitness function for $x_{new1}, x_{new2}, x_{new3}$.
  Update the HM according to $x_{new1}, x_{new2}, x_{new3}$ compared with the worst solution in the HM.
  iteration = iteration + 1.
  Update the best harmony (optimal global solution).
end while

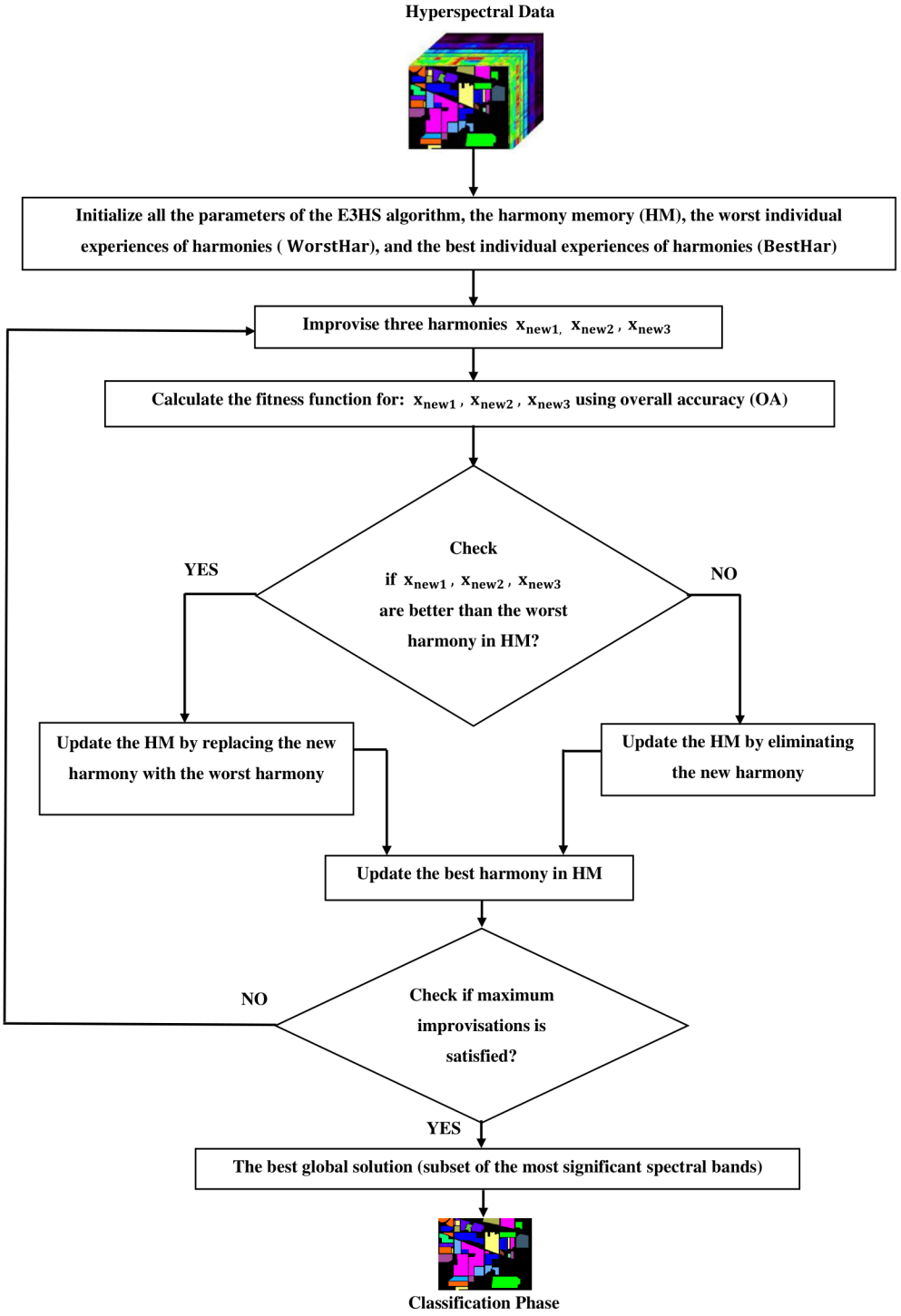

Figure 3. Workflow of the proposed method.

4. Experimental results

This section discusses the hyperspectral benchmark datasets used in this study. Moreover, the convergence behavior is analyzed for different numbers of spectral bands (5, 10, 15, 20) in order to determine the optimal number of bands with less complexity and outstanding classification performance. Additionally, the analytical classification results for the proposed method and the state-of-the-art methods are discussed for three real hyperspectral datasets.

4.1. Datasets

Three benchmark datasets were employed in this study to evaluate the performance of the E3HS approach compared to competing optimization algorithms (BA, AOA, PSO, HS, GA, and KH), which are the Indian Pines (IP), Pavia University (PU), and Salinas (SA) datasets. Figures 4a, 4b, and 4c demonstrate the ground truth of the Indian Pines dataset (which consists of 16 classes), the Pavia University dataset (which consists of 9 classes), and the Salinas dataset (which consists of 16 classes), respectively. Table 3 presents information about the datasets utilized in this study.

Table 3. Details of the datasets used in this study.

Dataset	Size	Spectral range	Spectral bands	Area	Sensor	Spatial resolution
Indian Pines	145*145 pixels	[0.4, 2.5] µm	200	Northwestern Indiana	AVIRIS	20 m
Pavia University	610*340 pixels	[0.43, 0.86] µm	103	Northern Italy	ROSIS	1.3 m
Salinas	512*217 pixels	[0.4, 2.5] µm	204	Southern California	AVIRIS	3.7 m

4.2. Convergence behavior analysis

In this section, convergence behavior is explored for the proposed method compared to the state-of-the-art methods by analyzing different numbers of spectral bands (5, 10, 15, and 20). Overall accuracy was calculated to evaluate the goodness of the solutions for the proposed method and all the state-of-the-art methods (BA [45], AOA [46], PSO [47], HS [43], GA [48], and KH [40]). Moreover, the convergence behavior was analyzed by plotting the fitness function (overall accuracy) against the number of iterations. More specifically, overall accuracy is calculated for the proposed method and the competing algorithms in each iteration using the SVM classifier. The E3HS approach demonstrated significant performance in terms of convergence behavior by selecting the best discriminative spectral bands compared to competing algorithms for different numbers of spectral bands.

Figures 5a, 5b, 5c, and 5d illustrate the convergence behavior over 100 runs for 5 spectral bands, 10 spectral bands, 15 spectral bands, and 20 spectral bands on the Indian Pines dataset, respectively. The overall accuracy is equal to 67.66%, 75.67%, 78.48%, and 79.13% for 5 spectral bands, 10 spectral bands, 15 spectral bands, and 20 spectral bands, respectively. Moreover, Figure 5 shows the significant improvement of E3HS by reaching the optimal global solution within the search space with the best overall accuracy compared to the competing algorithms.

Additionally, Figures 6a, 6b, 6c, and 6d display the convergence behavior over 100 runs for 5 spectral bands, 10 spectral bands, 15 spectral bands, and 20 spectral bands on the Pavia University dataset, respectively. The overall accuracy is equal to 85.46%, 88.13%, 89.32%, and 89.53% for 5 spectral bands, 10 spectral bands,

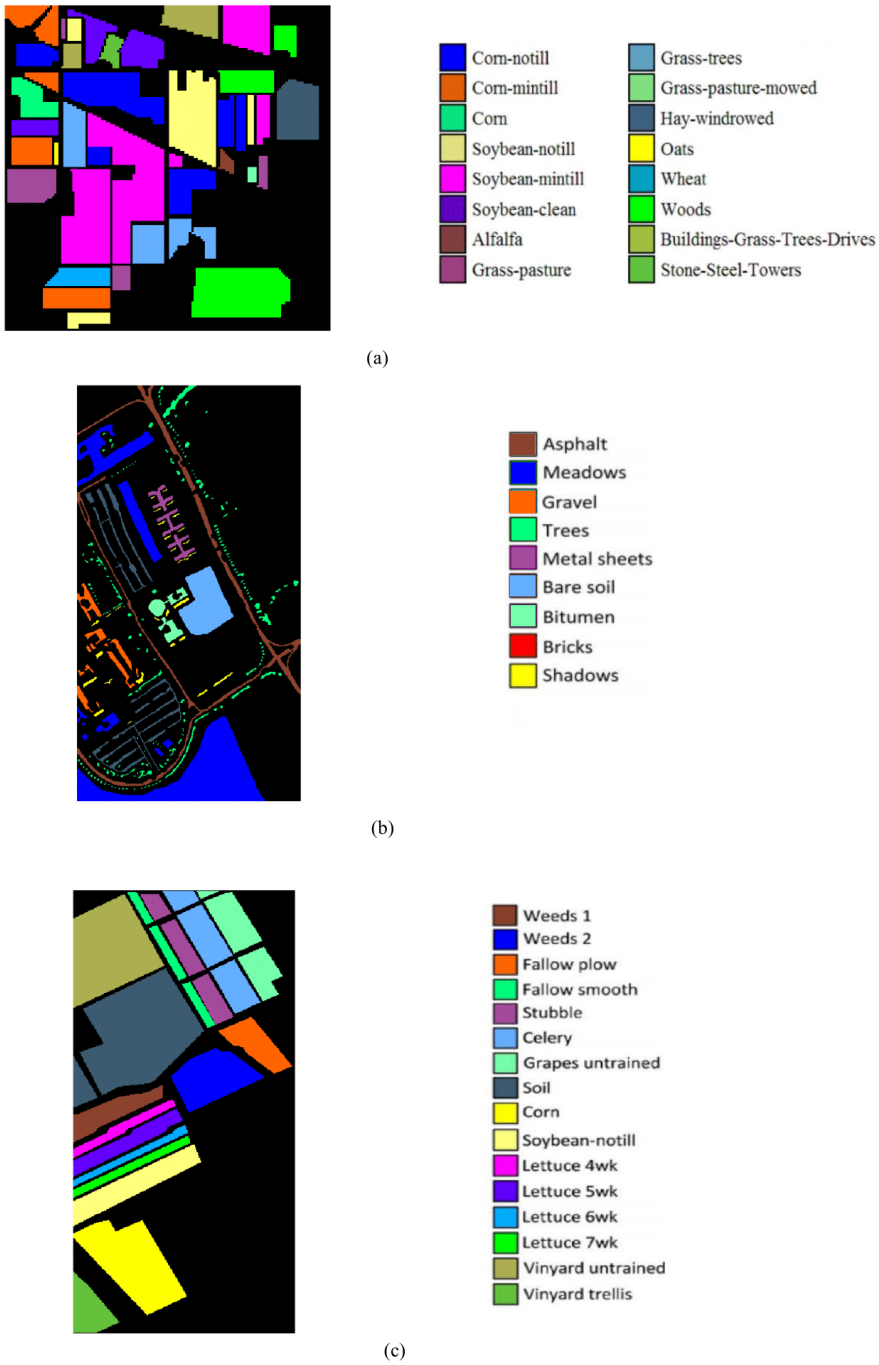

Figure 4. Ground truth for three hyperspectral datasets: (a) Indian Pines; (b) Pavia University; (c) Salinas.

15 spectral bands, and 20 spectral bands, respectively. Figure 5 shows that E3HS outperforms the competing methods by selecting the best relevant spectral bands compared to the state-of-the-art methods.

Finally, Figures 7a, 7b, 7c, and 7d exhibit the convergence behavior over 100 runs for 5 spectral bands, 10 spectral bands, 15 spectral bands, and 20 spectral bands on the Salinas University dataset, respectively. The

overall accuracy is equal to 90.11%, 91.24%, 91.72%, and 91.98% for 5 spectral bands, 10 spectral bands, 15 spectral bands, and 20 spectral bands, respectively. Figure 7 indicates the effectiveness of E3HS in reaching the best global solution and avoiding falling into the local optimum compared to the competing algorithms.

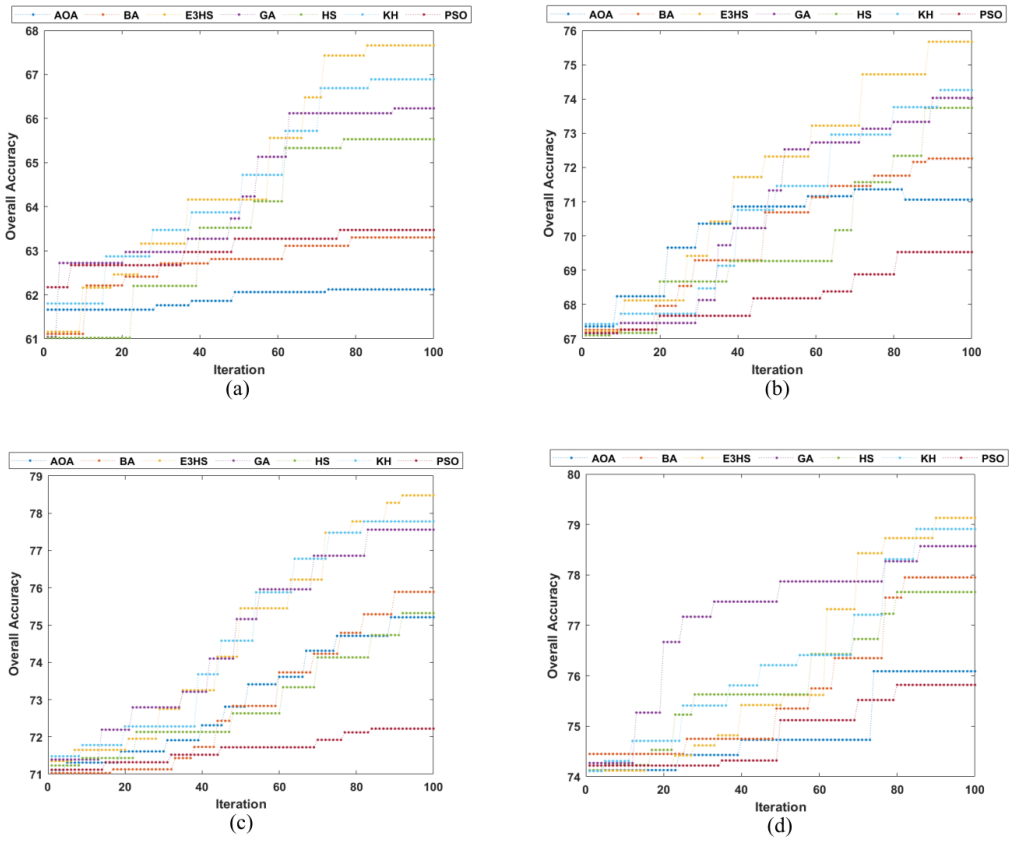

Figure 5. Convergence behavior for the Indian Pines dataset: (a) 5 spectral bands, (b) 10 spectral bands, (c) 15 spectral bands, (d) 20 spectral bands.

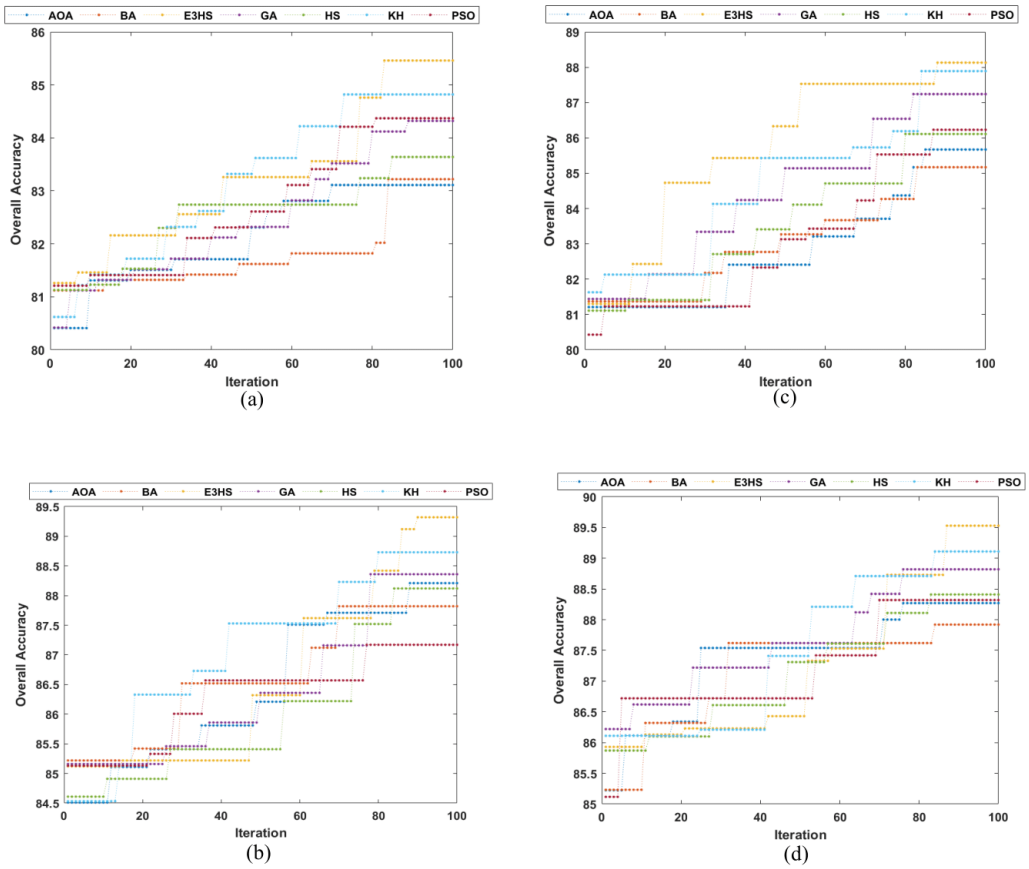

Figure 6. Convergence behavior for the Pavia University dataset: (a) 5 spectral bands, (b) 10 spectral bands, (c) 15 spectral bands, (d) 20 spectral bands.

4.3. Analytical results

This section presents the classification results for the proposed method and the state-of-the-art methods. Moreover, four standard evaluation metrics have been employed to evaluate the performance of the proposed method and the competing methods. These evaluation metrics are defined in Eqs. (6), (7), (8), and (9) for individual class accuracy (ICA), overall accuracy (OA), average accuracy (AA), and the kappa coefficient (KC), respectively.

$$ICA = \frac{C_{ij}}{T_i} \tag{6}$$

$$OA = \frac{\sum C_{ij}}{N} \tag{7}$$

$$AA = \frac{\sum_{i=1}^{M} ICA_i}{M} \tag{8}$$

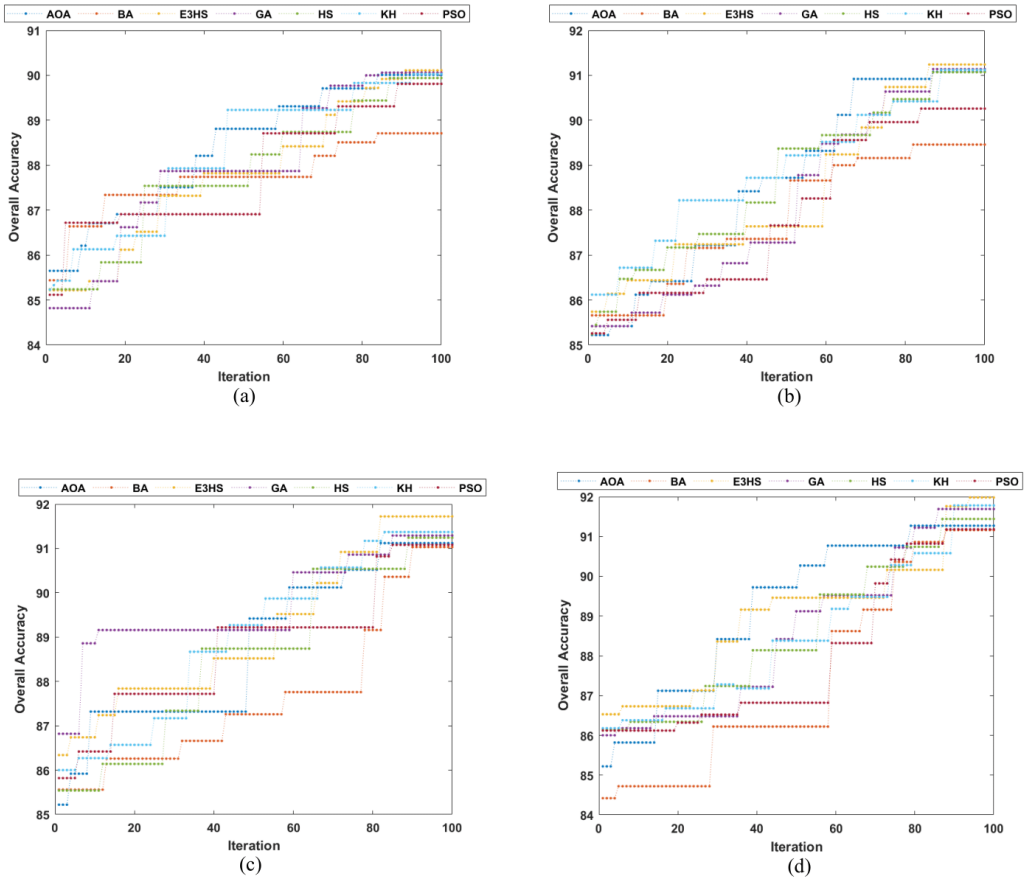

Figure 7. Convergence behavior for the Salinas dataset: (a) 5 spectral bands, (b) 10 spectral bands, (c) 15 spectral bands, (d) 20 spectral bands.

$$KC = \frac{N * \sum_{i,j=1}^{M} C_{ij} - \sum_{i,j=1}^{M} T_i * U_j}{N^2 - \sum_{i,j=1}^{M} T_i * U_j} \tag{9}$$

Here, C_{ij} represents the total number of correctly classified pixels in row i and column j of the confusion matrix, and T_i represents the total number of pixels in row i of the confusion matrix. N represents the total number of pixels, M indicates the total number of classes, and U_j indicates the total number of pixels in column j of the confusion matrix.

Table 4 illustrates the overall accuracy of the proposed method and the state-of-the-art after 100 iterations by considering four different numbers of spectral bands (5 spectral bands, 10 spectral bands, 15 spectral bands, and 20 spectral bands). The proposed method has significantly outperformed the competing methods for the three hyperspectral datasets as demonstrated in Table 4. More importantly, Table 4 shows the significant improvement of the proposed method for 15 selected spectral bands compared to 5 spectral bands and 10 spectral bands. On the other hand, Table 4 indicates little improvement for the proposed method and the competing methods among the other selected bands (15 and 20 spectral bands). The classification results are

Table 4. Overall accuracy for the proposed method and the state-of-the-art after 100 iterations on different numbers of spectral bands (in %).

Dataset	Optimization method	5 spectral bands	10 spectral bands	15 spectral bands	20 spectral bands
Indian Pines	BA	63.3	72.26	75.89	77.95
	AOA	62.12	71.06	75.21	76.09
	PSO	63.47	69.53	72.22	75.82
	HS	65.53	73.74	75.32	77.66
	GA	66.23	74.03	77.56	78.57
	KH	66.89	74.26	77.78	78.91
	E3HS	**67.66**	**75.67**	**78.48**	**79.13**
Pavia University	BA	83.22	85.17	87.82	87.92
	AOA	83.11	85.67	88.21	88.27
	PSO	84.37	86.23	87.17	88.32
	HS	83.64	86.11	88.12	88.41
	GA	84.32	87.24	88.36	88.82
	KH	84.82	87.89	88.73	89.11
	E3HS	**85.46**	**88.13**	**89.32**	**89.53**
Salinas	BA	88.71	89.46	91.03	91.16
	AOA	90.01	91.08	91.12	91.27
	PSO	89.81	90.26	91.08	91.18
	HS	89.94	91.07	91.24	91.44
	GA	90.06	91.14	91.29	91.69
	KH	90.03	91.12	91.37	91.78
	E3HS	**90.11**	**91.24**	**91.72**	**91.98**

considered for 15 spectral bands in this study for the proposed method and the state-of-the-art methods. Table 5 shows the 15 most relevant and significant bands for the proposed method and the state-of-the-art methods for the three hyperspectral datasets.

Table 6 illustrates the classification results for E3HS and the competing methods using two machine learning classifiers (KNN and SVM) on the Indian Pines dataset. Moreover, Table 6 shows the best accuracy values (in bold) for all optimization techniques. Furthermore, four performance metrics are shown in Table 6, which are ICA, OA, AA, and KC. The ICA is shown for E3HS and the state-of-the-art methods with 16 classes. Table 6 also reveals the significant superiority of the E3HS model compared to the state-of-the-art methods with OA equal to 77.68% using KNN and 87.49% using SVM. On the other hand, the OA for the competing methods ranges between 71.42% and 76.95% using KNN and 82.13% and 85.70% using SVM.

Similarly, Table 7 shows the outstanding performance of E3HS and the competing methods using KNN and SVM on the Pavia University dataset. The ICA is shown for E3HS and the state-of-the-art methods with 9 classes. Furthermore, Table 7 shows the outstanding performance of the E3HS model compared to the state-of-the-art methods with OA equal to 90.44% using KNN and 94.85% using SVM. On the other hand, the OA for the competing methods ranges between 86.57% and 88.56% using KNN and 90.92% and 93.90% using SVM.

Finally, Table 8 demonstrates the effectiveness of the E3HS model in selecting the most informative spectral bands compared to the competing methods on the Salinas dataset. The ICA is presented for E3HS and the state-of-the-art methods with 16 classes in Table 8. Moreover, Table 8 displays the considerable improvement of the E3HS model compared to the state-of-the-art methods with OA equal to 90.55% using KNN and 94.41% using SVM. On the other hand, the OA for the competing methods ranges between 90% and 90.30% using KNN and 93.24% and 94% using SVM.

Table 5. The 15 most relevant and significant bands for three hyperspectral datasets.

Dataset	Optimization method	Selected spectral bands
Indian Pines	BA	17,59,187,41,112,100,7,170,182,130,37,117,90,35,21
	AOA	18,149,53,115,63,57,118,43,98,36,127,89,39,46,175
	PSO	78,107,134,112,166,59,26,52,129,176,88,154,36,41,54
	HS	175,137,119,35,64,42,127,74,28,114,138,16,8,17,20
	GA	68,126,122,37,178,30,7,18,28,35,20,166,82,39,42
	KH	37,131,17,34,154,46,160,177,178,68,172,149,82,66,127
	E3HS	26,44,149,34,176,20,161,98,6,128,81,64,35,39,68
Pavia University	BA	16,84,85,43,65,75,82,53,68,21,6,67,97,23,64
	AOA	12,17,42,63,72,82,52,68,21,6,66,92,23,64,33
	PSO	38,81,46,18,94,52,49,61,24,66,69,83,8,19,71
	HS	80,37,7,87,48,102,22,99,69,85,75,17,73,13,2
	GA	68,23,25,85,19,83,87,18,5,36,3,8,66,9,71
	KH	81,97,68,6,83,43,6,25,87,63,64,62,69,91,14
	E3HS	44,18,77,19,103,83,85,68,41,20,60,99,87,41,69
Salinas	BA	44,8,78,163,151,87,41,20,17,26,171,37,10,36,33
	AOA	162,20,56,5,112,16,61,27,86,52,64,45,153,37,121
	PSO	82,28,104,136,51,101,115,80,66,93,44,120,54,34,8
	HS	61,25,70,173,17,96,4,9,40,42,51,37,140,10,33
	GA	164,17,30,20,19,65,55,37,137,48,16,18,91,83,28
	KH	19,21,5,68,52,28,44,87,56,37,165,87,14,52,47
	E3HS	47,66,34,51,39,46,37,27,63,65,87,20,32,8,167

Figures 8, 9, and 10 provide the classification maps for the Indian Pines, Pavia University, and Salinas datasets, respectively. These figures show the significant improvement for the E3HS model in terms of smoothness and a smaller number of misclassifications compared to the competing algorithms due to the effectiveness of E3HS in selecting the most relevant and informative spectral bands.

Table 6. Classification accuracy (%) for E3HS compared with the competing algorithms for the Indian Pines dataset.

Class Number	Class name	KNN							SVM						
		BA	AOA	PSO	HS	GA	KH	E3HS	BA	AOA	PSO	HS	GA	KH	E3HS
1	Alfalfa	63.33	44.68	46.67	**76**	66.67	51.28	70.59	70	90.91	88.89	**96.97**	75.56	80.95	93.94
2	Corn-notill	**69.44**	62.21	60.36	65.11	66.31	66.35	68.61	83.97	79.61	73.49	80.68	81.82	82.38	**87.26**
3	Corn-mintill	64.22	69.35	65.43	61.09	72.09	**78.77**	68.51	81.28	80.63	79.23	80.73	82.81	**83.78**	83.72
4	Corn	60.16	54.78	55	57.55	60.68	60.68	**63.46**	69.95	**77.84**	70.09	72.38	72.57	72.06	72.32
5	Grass-pasture	81.48	**88.36**	77.17	83.85	82.25	83.24	**88.36**	89.39	93.19	86.60	86.07	**93.97**	88.89	92.89
6	Grass-trees	**86.44**	79.72	81.36	80.03	79.63	83.03	83.06	92.86	90.82	**92.97**	90.91	92.74	92.08	92.88
7	Grass-pasture-mowed	94.74	87.50	71.43	83.33	**100**	91.67	94.74	90.91	82.61	66.67	90.91	**100**	**100**	80
8	Hay-windrowed	92.14	92.53	93.62	**93.83**	92.46	91.98	91.77	97.89	97.92	95.48	97.69	**98.95**	98.94	98.44
9	Oats	37.50	**100**	**100**	80	50	**100**	**100**	**90.91**	75	83.33	77.78	75	78.57	66.67
10	Soybean-notill	67.34	65.45	60.32	68.03	69.32	71.30	**71.72**	79.31	77.02	74.69	76.97	**87.06**	82.31	80.17
11	Soybean-mintill	76.49	76.20	69.84	76.14	76.94	77.16	**77.93**	82.62	80.13	78.91	83.93	81.57	81.96	**85.09**
12	Soybean-clean	62.95	56.49	52.79	**66.47**	65.46	63.79	65.10	85.46	**90.31**	82.28	81.30	78.12	86.72	88.27
13	Wheat	84.95	83.78	83.33	80.71	**88.24**	83.06	82.42	93.14	92.57	90.96	91.48	87.98	92.61	**96.32**
14	Woods	90.94	**91.01**	87.16	89.15	88.94	87.80	90.04	92.79	92.37	91.57	94.59	92.63	93.62	**95.08**
15	Buildings-Grass-Trees-Drives	72.46	73.95	70.83	66.43	**83.33**	68.83	66.06	74.14	80.43	**83.26**	83.19	74.18	74.71	77.27
16	Stone-Steel-Towers	**100**	98.48	**100**	98.36	**100**	96.72	98.46	93.24	98.55	98.55	97.18	**100**	97.06	**100**
OA		76.45	74.95	71.42	75.16	76.78	76.95	**77.68**	85.34	84.61	82.13	85.09	85.42	85.70	**87.49**
AA		75.29	76.53	73.46	76.63	77.64	78.48	**80.05**	85.49	86.24	83.56	86.42	85.94	86.67	**86.90**
KC		73.09	71.31	67.20	71.58	73.40	73.58	**74.42**	83.25	82.38	79.57	82.98	83.29	83.66	**85.72**

5. Discussion

In this study, the E3HS model has been introduced to select the most significant spectral bands in order to decrease the calculation complexity and eliminate the Hughes phenomenon. Specifically, the proposed method aims to create a balance between exploration and exploitation strategies by including two extra solutions in each iteration. The first one considers the mean of the worst individual experiences for all solutions in the

Table 7. Classification accuracy (%) for E3HS compared with the competing algorithms for the Pavia University dataset.

Class Number	Class Name	KNN							SVM						
		BA	AOA	PSO	HS	GA	KH	E3HS	BA	AOA	PSO	HS	GA	KH	E3HS
1	Asphalt	91.97	92.59	92.04	91.08	91.60	92.52	**93.82**	93.87	94.28	93.13	93.92	94.12	94.12	**94.85**
2	Meadows	86.93	87.91	86.21	86.79	87.81	89.19	**90.75**	95.22	94.67	92.25	94.76	95.26	96.26	**96.79**
3	Gravel	73.42	71.38	75.41	67.83	72.30	73.73	**77.81**	81.38	86.13	84.57	83.19	**87.06**	85.16	85.02
4	Trees	95.81	95.16	95.27	**97.26**	95.42	96.64	96.61	96.54	96.08	95.61	96.72	94.97	**97.15**	96.64
5	Painted metal sheets	99.44	98.89	97.98	99.44	98.24	**99.53**	**99.53**	**99.91**	99.63	98.25	98.80	**99.91**	99.26	**99.91**
6	Bare Soil	81.68	82.70	81.50	84.37	85.13	86.99	**89.93**	89.83	90.04	85.79	91.58	89.82	91.83	**93.94**
7	Bitumen	74.74	76.31	77.88	76.87	73.82	76.14	**82.67**	81.68	86.14	83.53	86.55	86.64	86.30	**88.92**
8	Self-Blocking Bricks	78.11	78.35	79.73	79.10	78.83	80.39	**83.38**	86.48	85.30	84.13	84.46	86.17	85.66	**89.08**
9	Shadows	**100**	**100**	**100**	**100**	**100**	**100**	99.87	**100**	**100**	**100**	**100**	**100**	99.87	**100**
OA		86.63	87.19	86.57	86.65	87.23	88.56	**90.44**	92.85	92.97	90.92	92.96	93.25	93.90	**94.85**
AA		86.90	87.03	87.34	86.97	87.02	88.35	**90.49**	91.66	92.47	90.81	92.22	92.66	92.84	**93.91**
KC		81.92	82.72	81.81	81.90	82.73	84.58	**87.15**	90.49	90.63	87.87	90.62	91.02	91.89	**93.16**

Table 8. Classification accuracy (%) for E3HS compared with the competing algorithms for the Salinas dataset.

Class Number	Class Name	KNN							SVM						
		BA	AOA	PSO	HS	GA	KH	E3HS	BA	AOA	PSO	HS	GA	KH	E3HS
1	Brocoli_green_weeds_1	99.94	**100**	**100**	**100**	**100**	**100**	**100**	99.75	**100**	**100**	**100**	**100**	99.81	99.94
2	Brocoli_green_weeds_2	98.77	99.36	99.30	**99.53**	99.37	99.27	99.23	99.60	99.77	99.60	**99.90**	99.80	99.63	**99.90**
3	Fallow	93.27	92.54	**95.35**	91.92	94.34	93.25	94.35	97.38	98.55	98.68	98.67	97.70	98.86	**98.98**
4	Fallow_ rough_ plow	98.14	96.52	97.54	**98.41**	98.32	97.71	97.63	98.67	99.20	98.92	98.93	**99.28**	98.58	99.11
5	Fallow_ smooth	98.81	**99.18**	98.53	98.81	98.96	99	99.09	97.25	**99.25**	98.83	98.92	99.01	98.83	98.47
6	Stubble	99.94	99.97	99.91	**100**	99.97	99.97	99.97	**100**	99.97	99.94	99.87	99.97	**100**	99.94
7	Celery	99.41	99.86	99.69	99.75	**100**	99.58	99.86	99.76	99.69	99.72	99.69	99.86	**100**	99.83
8	Grapes_ untrained	77.74	77.33	77.21	77.41	77.51	**78.27**	78.16	83.64	84.77	84.81	**85.78**	85.23	83.91	85.70
9	Soil_ vinyard_ develop	98.63	98.50	99.04	98.73	**99.10**	97.81	98.50	99.38	99.36	99.36	99.01	99.18	**99.54**	**99.54**
10	Corn_ senesced_ green_ weeds	93.75	**94.39**	92.01	91.19	91.72	93.90	91.44	97.24	97.53	97.17	96.26	97.56	97.43	**97.59**
11	Lettuce_romaine_4wk	89.89	88.70	93.47	89.98	**93.54**	84.70	92.35	96.46	**99.18**	96.99	95.02	98.13	98.15	97.80
12	Lettuce_romaine_5wk	96.31	**97.16**	96.17	96.42	97.65	96.42	96.85	99.03	**99.93**	99.61	99.68	99.48	99.48	99.68
13	Lettuce_romaine_6wk	93.82	96.34	**97.29**	95.98	95.32	94.62	95.76	98.37	99.32	99.04	98.78	99.59	**99.73**	**99.73**
14	Lettuce_romaine_7wk	96.47	94.15	**97.12**	95.61	95.95	96.79	95.76	97.20	98.72	96.37	98.25	97.91	**99.76**	98.36
15	Vinyard_ untrained	70.84	71.95	70.53	73.19	71.11	73.08	**73.44**	80.66	80.46	80.46	81.79	82.11	83.62	**83.89**
16	Vinyard_ vertical_ trellis	99.09	99.08	99.51	98.68	98.95	99.44	**99.79**	99.10	**99.65**	98.76	**99.65**	98.89	99.45	99.38
OA		90	90.12	90.09	90.20	90.23	90.30	**90.55**	93.24	93.79	93.62	93.95	93.99	94	**94.41**
AA		94.05	94.07	94.54	94.10	94.49	93.99	**94.51**	96.47	97.21	96.77	96.89	97.11	97.30	**97.36**
KC		88.86	88.99	88.96	89.07	89.12	89.19	**89.47**	92.46	93.08	92.89	93.26	93.31	93.31	**93.77**

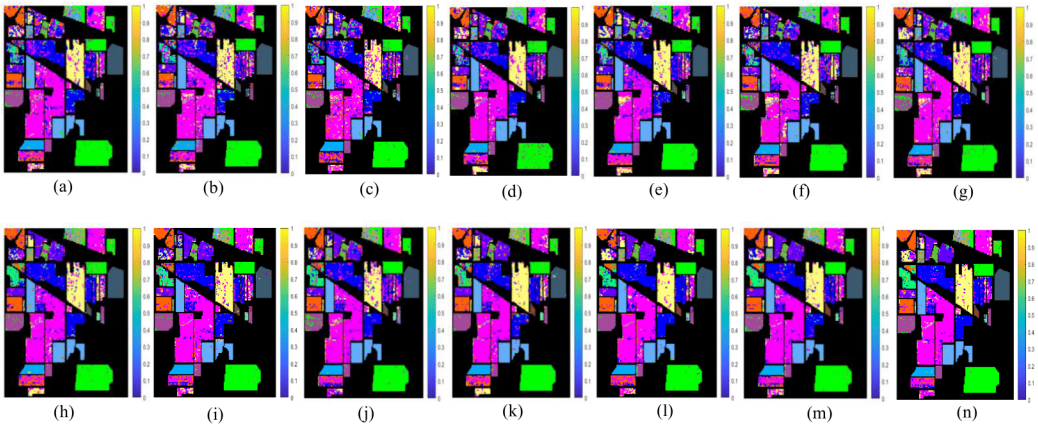

Figure 8. Classification map for Indian Pines dataset using: (a) BA-KNN; (b) AOA-KNN; (c) PSO-KNN; (d) HS-KNN; (e) GA-KNN; (f) KH-KNN; (g) E3HS-KNN; (h) BA-SVM; (i) AOA-SVM; (j) PSO-SVM; (k) HS-SVM; (l) GA-SVM; (m) KH-SVM; (n) E3HS-SVM.

HM. On the other hand, the second one considers the mean of the best individual experiences for all solutions in the HM. Consequently, both the global search and the local search are improved effectively. Moreover, the

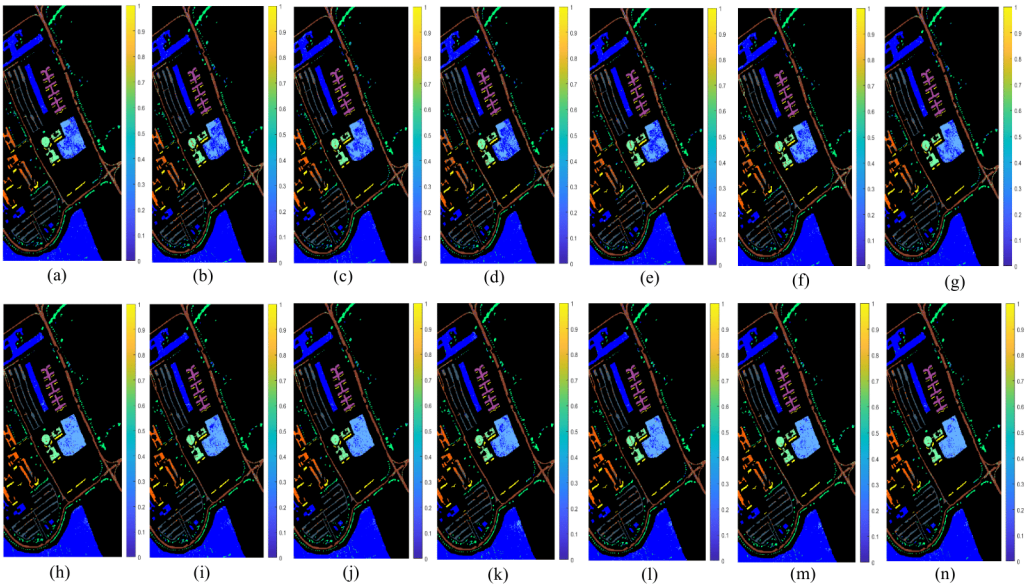

Figure 9. Classification map for Pavia University dataset using: (a) BA-KNN; (b) AOA-KNN; (c) PSO-KNN; (d) HS-KNN; (e) GA-KNN; (f) KH-KNN; (g) E3HS-KNN; (h) BA-SVM; (i) AOA-SVM; (j) PSO-SVM; (k) HS-SVM; (l) GA-SVM; (m) KH-SVM; (n) E3HS-SVM.

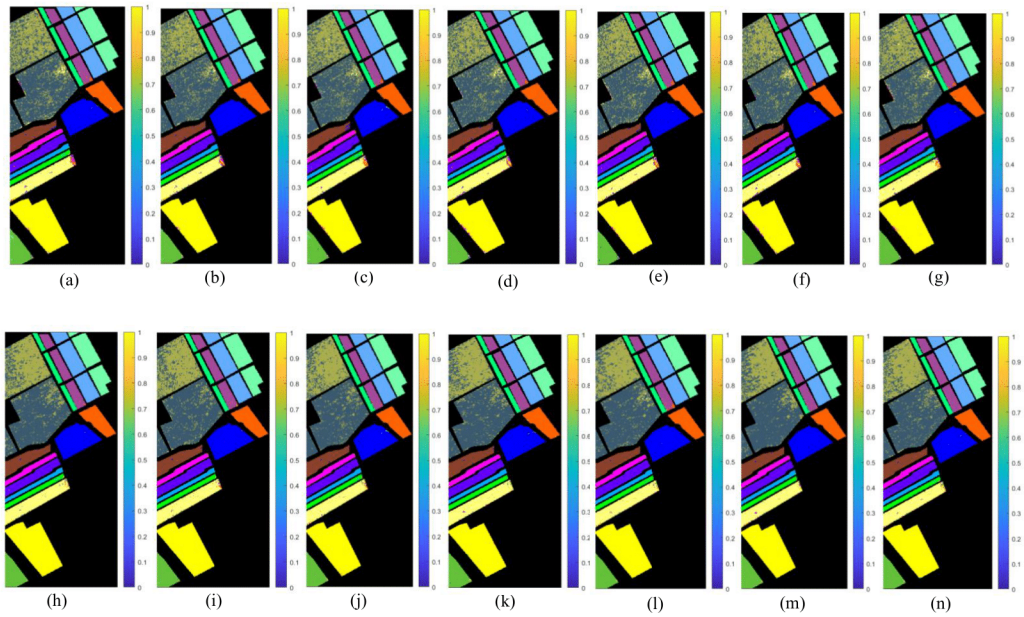

Figure 10. Classification map for Salinas dataset using: (a) BA-KNN; (b) AOA-KNN; (c) PSO-KNN; (d) HS-KNN; (e) GA-KNN; (f) KH-KNN; (g) E3HS-KNN; (h) BA-SVM; (i) AOA-SVM; (j) PSO-SVM; (k) HS-SVM; (l) GA-SVM; (m) KH-SVM; (n) E3HS-SVM.

proposed method can avoid falling into local optima and reach the optimal global solution within the search space efficiently. Additionally, the proposed work has been compared with six competing optimization techniques:

BA, AOA, PSO, HS, GA, and KH. The proposed method and all the state-of-the-art methods were executed using MATLAB R2021b with 8 GB RAM in Windows 11. Moreover, 10% per class was randomly selected as the training samples for the proposed method and the state-of-the-art methods, and the remainder was used for the testing samples. Furthermore, two machine learning classifiers (KNN and SVM) were employed at the pixel level to perform the classification phase using the selected spectral bands. Five-fold cross-validation was performed on the training data for the SVM classifier, and the KNN classifier considered the five nearest neighbors (K = 5) for classification. However, spatial features that represent strong relationships between neighboring pixels were not incorporated within the classification phase, which is considered as the weakness of the proposed method.

6. Conclusion

The Hughes phenomenon is a notable challenge that arises due to the high dimensionality of HSIs. Therefore, it is crucial to perform dimensionality reduction on HSIs in order to mitigate the processing time and computational complexities. This paper has introduced the E3HS algorithm for the selection of the most discriminative spectral bands in HSIs. The new algorithm improves upon the existing HS algorithm by incorporating two additional solutions respectively derived from the best and worst individual experiences of the harmonies. The first solution exploits the worst individual experiences of the harmonies. This strategy introduces an element of exploration, allowing the algorithm to overcome premature convergence. Conversely, the second solution leverages the best individual experiences of the harmonies, aiming to enhance the exploitation phase. By considering the knowledge gained from successful harmonies, this approach seeks to identify and prioritize the most informative bands. By incorporating these two additional solutions, the E3HS algorithm strikes a balance between exploration and exploitation, enabling a more comprehensive search for the most discriminative spectral bands. The proposed algorithm offers an improved approach for hyperspectral band selection, addressing the limitations associated with existing methods and enhancing the overall performance of the band selection process. Consequently, the proposed E3HS algorithm achieves the optimal global solution by effectively navigating the HM and avoiding getting trapped in local optima. This capability ensures that the algorithm converges rapidly toward the best possible subset of the most informative bands. The ability to reach the optimal global solution within the HM is a significant achievement of the E3HS algorithm. It enhances the efficiency and effectiveness of hyperspectral band selection by ensuring that the selected subset of bands is truly informative and discriminative. Finally, two machine learning classifiers (KNN and SVM) have been employed for HSI classification at the pixel level on the selected spectral bands. The proposed E3HS algorithm exhibited substantial improvements when compared to six competing algorithms: the bat algorithm (BA), Archimedes optimization algorithm (AOA), particle swarm optimization (PSO), harmony search (HS), genetic algorithm (GA), and krill herd (KH). In the course of rigorous experimentation and comparative analysis, the E3HS algorithm consistently outperformed these competing algorithms in terms of both convergence speed and the quality of the selected spectral bands. By leveraging the diversity and knowledge gained from successful and unsuccessful harmonies, the E3HS algorithm showcased a higher degree of robustness and efficiency in selecting the most informative bands. In future work, we plan to apply the proposed method to other benchmark datasets of HSIs to further validate its effectiveness in selecting significant discriminative spectral bands. To enhance the optimization process and accelerate the convergence towards the optimal global solution, we will explore the use of hybrid optimization

algorithms. Combining multiple optimization techniques can leverage their respective strengths and overcome their limitations, leading to more efficient and effective band selection. Additionally, selecting an appropriate fitness function tailored to the specific classification task can further enhance the algorithm's performance and ensure the selection of the most relevant spectral bands. Moreover, it is important to acknowledge that HSIs contain not only spectral information but also valuable spatial information. In our future work, we aim to incorporate and exploit this spatial information in the classification process. By integrating spatial features or employing spatial-spectral methods, we can capture spatial dependencies and contextual information, leading to improved classification results. This holistic approach will enhance the overall performance of HSI classification and enable a more comprehensive analysis of the data.

References

[1] Elmasry G, Barbin DF, Sun DW, Allen P. Meat quality evaluation by hyperspectral imaging technique: an overview. Critical Reviews in Food Science and Nutrition 2012; 52 (8): 689-711. https://doi.org/10.1080/10408398.2010.507908

[2] He X, Chen Y, Lin Z. Spatial-spectral transformer for hyperspectral image classification. Remote Sensing 2021; 13 (3): 498. https://doi.org/10.3390/rs13030498

[3] Zhong Z, Li J, Luo Z, Chapman M. Spectral–spatial residual network for hyperspectral image classification: a 3-D deep learning framework. IEEE Transactions on Geoscience and Remote Sensing 2017; 56 (2): 847-858. https://doi.org/10.1109/TGRS.2017.2755542

[4] Sethy PK, Pandey C, Sahu YK, Behera SK. Hyperspectral imagery applications for precision agriculture - a systemic survey. Multimedia Tools and Applications 2022; 81: 3005-3038. https://doi.org/10.1007/s11042-021-11729-8

[5] Stuart MB, Davies M, Hobbs MJ, Pering TD, McGonigle AJ et al. High-resolution hyperspectral imaging using low-cost components: application within environmental monitoring scenarios. Sensors 2022; 22 (12): 4652. https://doi.org/10.3390/s22124652

[6] Peyghambari S, Zhang Y. Hyperspectral remote sensing in lithological mapping, mineral exploration, and environmental geology: an updated review. Journal of Applied Remote Sensing 2021; 15 (3): 031501. https://doi.org/10.1117/1.JRS.15.031501

[7] Leavesley SJ, Sweat B, Abbott C, Favreau PF, Annamdevula NS et al. Comparing methods for analysis of biomedical hyperspectral image data. Proceedings of SPIE - Imaging, Manipulation, and Analysis of Biomolecules, Cells, and Tissues 2017; 15: 10068. https://doi.org/10.1117/12.2252827

[8] Cucci C, Picollo M, Chiarantini L, Uda G, Fiori L et al. Remote-sensing hyperspectral imaging for applications in archaeological areas: non-invasive investigations on wall paintings and on mural inscriptions in the Pompeii site. Microchemical Journal 2020; 158: 105082. https://doi.org/10.1016/j.microc.2020.105082

[9] Ma Y, Wu H, Wang L, Huang B, Ranjan R et al. Remote sensing big data computing: challenges and opportunities. Future Generation Computer Systems 2015; 51: 47-60. https://doi.org/10.1016/j.future.2014.10.029

[10] Moharram MA, Sundaram DM. Dimensionality reduction strategies for land use land cover classification based on airborne hyperspectral imagery: a survey. Environmental Science and Pollution Research 2023; 30 (3): 5580-5602. https://doi.org/10.1007/s11356-022-24202-2

[11] Jiang J, Ma J, Chen C, Wang Z, Cai Z et al. SuperPCA: A superpixelwise PCA approach for unsupervised feature extraction of hyperspectral imagery. IEEE Transactions on Geoscience and Remote Sensing 2018; 56 (8): 4581-4593. https://doi.org/10.1109/TGRS.2018.2828029

[12] Xia J, Bombrun L, Adalı T, Berthoumieu Y, Germain C. Spectral–spatial classification of hyperspectral images using ICA and edge-preserving filter via an ensemble strategy. IEEE Transactions on Geoscience and Remote Sensing 2016; 54 (8): 4971-4982. DOI: 10.1109/TGRS.2016.2553842

[13] Chakravarty S, Mishra R, Ransingh A, Dash S, Mohanty SN et al. Feature extraction and classification of hyperspectral imaging using minimum noise fraction and deep convolutional neural network. Journal of Electronic Imaging 2023; 32 (2): 021610. https://doi.org/10.1117/1.JEI.32.2.021610

[14] Zhao W, Du S. Spectral–spatial feature extraction for hyperspectral image classification: a dimension reduction and deep learning approach. IEEE Transactions on Geoscience and Remote Sensing 2016; 54 (8): 4544-4554. https://doi.org/10.1109/TGRS.2016.2543748

[15] Yang D, Bao W. Group lasso-based band selection for hyperspectral image classification. IEEE Geoscience and Remote Sensing Letters 2017; 14 (12): 2438-2442. https://doi.org/10.1109/LGRS.2017.2768074

[16] Serpico SB, Bruzzone L. A new search algorithm for feature selection in hyperspectral remote sensing images. IEEE Transactions on Geoscience and Remote Sensing 2001; 39 (7): 1360-1367. https://doi.org/10.1109/36.934069

[17] Persello C, Bruzzone L. Kernel-based domain-invariant feature selection in hyperspectral images for transfer learning. IEEE Transactions on Geoscience and Remote Sensing 2015; 54 (5): 2615-2626. https://doi.org/10.1109/TGRS.2015.2503885

[18] Chang CI, Kuo YM, Chen S, Liang CC, Ma KY et al. Self-mutual information-based band selection for hyperspectral image classification. IEEE Transactions on Geoscience and Remote Sensing 2020; 59 (7): 5979-5997. https://doi.org/10.1109/TGRS.2020.3024602

[19] Feng J, Jiao L, Liu F, Sun T, Zhang X. Mutual-information-based semi-supervised hyperspectral band selection with high discrimination, high information, and low redundancy. IEEE Transactions on Geoscience and Remote Sensing 2014; 53 (5): 2956-2969. https://doi.org/10.1109/TGRS.2014.2367022

[20] Bajcsy P, Groves P. Methodology for hyperspectral band selection. Photogrammetric Engineering and Remote Sensing 2004; 70: 793-802. https://doi.org/10.14358/PERS.70.7.793

[21] Moharram MA, Sundaram DM. Land use and land cover classification with hyperspectral data: a comprehensive review of methods, challenges and future directions. Neurocomputing 2023; 536: 90-113. https://doi.org/10.1016/j.neucom.2023.03.025

[22] Luo X, Shen Z, Xue R, Wan H. Unsupervised band selection method based on importance-assisted column subset selection. IEEE Access 2018; 7: 517-527. https://doi.org/10.1109/ACCESS.2018.2885545

[23] Zeng M, Ning B, Hu C, Gu Q, Cai Y et al. Hyper-graph regularized kernel subspace clustering for band selection of hyperspectral image. IEEE Access 2020; 8: 135920-135932. https://doi.org/10.1109/ACCESS.2020.3010519

[24] Ren Z, Zhai Q, Sun L. A novel method for hyperspectral mineral mapping based on clustering-matching and nonnegative matrix factorization. Remote Sensing 2022; 14 (4): 1042. https://doi.org/10.3390/rs14041042

[25] Xu B, Li X, Hou W, Wang Y, Wei Y. A similarity-based ranking method for hyperspectral band selection. IEEE Transactions on Geoscience and Remote Sensing 2021; 59 (11): 9585-9599. https://doi.org/10.1109/TGRS.2020.3048138

[26] Xie F, Li F, Lei C, Yang J, Zhang Y. Unsupervised band selection based on artificial bee colony algorithm for hyperspectral image classification. Applied Soft Computing 2019; 75: 428-440. https://doi.org/10.1016/j.asoc.2018.11.014

[27] Li S, Wu H, Wan D, Zhu J. An effective feature selection method for hyperspectral image classification based on genetic algorithm and support vector machine. Knowledge-Based Systems 2011; 24 (1): 40-48. https://doi.org/10.1016/j.knosys.2010.07.003

[28] Su H, Du Q, Chen G, Du P. Optimized hyperspectral band selection using particle swarm optimization. IEEE Journal of Selected Topics in Applied Earth Observations and Remote Sensing 2014; 7 (6): 2659-2670. https://doi.org/10.1109/JSTARS.2014.2312539

[29] Nakamura RY, Fonseca LMG, Dos Santos JA, Torres RDS, Yang XS et al. Nature-inspired framework for hyperspectral band selection. IEEE Transactions on Geoscience and Remote Sensing 2013; 52 (4): 2126-2137. https://doi.org/10.1109/TGRS.2013.2258351

[30] Sawant SS, Manoharan P. New framework for hyperspectral band selection using modified wind-driven optimization algorithm. International Journal of Remote Sensing 2019; 40 (20): 7852-7873. https://doi.org/10.1080/01431161.2019.1607609

[31] Anand R, Samiaappan S, Veni S, Worch E, Zhou M. Airborne hyperspectral imagery for band selection using moth–flame metaheuristic optimization. Journal of Imaging 2022; 8 (5): 126. https://doi.org/10.3390/jimaging8050126

[32] Jia S, Yuan Y, Li N, Liao J, Huang Q et al. A multiscale superpixel-level group clustering framework for hyperspectral band selection. IEEE Transactions on Geoscience and Remote Sensing 2022; 60: 5523418. https://doi.org/10.1109/TGRS.2022.3150361

[33] Chowdhury AR, Hazra J, Dasgupta K, Dutta P. Fuzzy rule-based hyperspectral band selection algorithm with ant colony optimization. Innovations in Systems and Software Engineering 2022: 1-14. https://doi.org/10.1007/s11334-021-00432-4

[34] Deepthi, Devassy BM, George S, Nussbaum P, Thomas T. Classification of forensic hyperspectral paper data using hybrid spectral similarity algorithms. Journal of Chemometrics 2022; 36 (1): e3387. https://doi.org/10.1002/cem.3387

[35] Sawant SS, Prabukumar M, Samiappan S. A modified Cuckoo Search algorithm based optimal band subset selection approach for hyperspectral image classification. Journal of Spectral Imaging 2020; 9: a6. https://doi.org/10.1255/jsi.2020.a6

[36] Sheikh KH, Ahmed S, Mukhopadhyay K, Singh PK, Yoon JH et al. EHHM: Electrical harmony based hybrid metaheuristic for feature selection. IEEE Access 2020; 8: 158125-158141. https://doi.org/10.1109/ACCESS.2020.3019809

[37] Medjahed SA, Saadi TA, Benyettou A, Ouali M. Gray wolf optimizer for hyperspectral band selection. Applied Soft Computing 2016; 40: 178-186. https://doi.org/10.1016/j.asoc.2015.09.045

[38] He C, Zhang Y, Gong D. A pseudo-label guided artificial bee colony algorithm for hyperspectral band selection. Remote Sensing 2020; 12 (20): 3456. https://doi.org/10.3390/rs12203456

[39] Manoharan P, Boggavarapu PKL. Improved whale optimization based band selection for hyperspectral remote sensing image classification. Infrared Physics & Technology 2021; 119: 103948. https://doi.org/10.1016/j.infrared.2021.103948

[40] Moharram MA, Sundaram DM. Spatial–spectral hyperspectral images classification based on Krill Herd band selection and edge-preserving transform domain recursive filter. Journal of Applied Remote Sensing 2022; 16 (4): 044508. https://doi.org/10.1117/1.JRS.16.044508

[41] Anand R, Samiaappan S, Veni S, Worch E, Zhou M. Airborne hyperspectral imagery for band selection using moth–flame metaheuristic optimization. Journal of Imaging 2022; 8 (5): 126. https://doi.org/10.3390/jimaging8050126

[42] Wei Y, Hu H, Xu H, Mao X. Unsupervised hyperspectral band selection via multimodal evolutionary algorithm and subspace decomposition. Sensors 2023; 23 (4): 2129. https://doi.org/10.3390/s23042129

[43] Geem ZW, Kim JH, Loganathan GV. A new heuristic optimization algorithm: harmony search. Simulation 2001; 76 (2): 60-68. https://doi.org/10.1177/003754970107600201

[44] Kim JH, Geem ZW, Kim ES. Parameter estimation of the nonlinear Muskingum model using harmony search. Journal of the American Water Resources Association 2001; 37 (5): 1131-1138. https://doi.org/10.1111/j.1752-1688.2001.tb03627.x

[45] Yang XS, Hossein Gandomi A. Bat algorithm: a novel approach for global engineering optimization. Engineering Computations 2012; 29 (5): 464-483. https://doi.org/10.1108/02644401211235834

[46] Hashim FA, Hussain K, Houssein EH, Mabrouk MS, Al-Atabany W. Archimedes optimization algorithm: a new metaheuristic algorithm for solving optimization problems. Applied Intelligence 2021; 51: 1531-1551. https://doi.org/10.1007/s10489-020-01893-z

[47] Kennedy J, Eberhart R. Particle swarm optimization. In: Proceedings of ICNN'95-International Conference on Neural Networks; Perth, Australia; 1995. pp. 1942-1948. https://doi.org/10.1109/ICNN.1995.488968

[48] Holland JH. Genetic algorithms. Scientific American 1992; 267 (1): 66-73.